ARMA 19-A-1568-ARMA

Comprehensive laboratory investigation and model fitting of Klinkenberg Effect and its role on apparent permeability in various U.S. shale formations

Zihao Li, Nino Ripepi, and Cheng Chen
Virginia Tech, Blacksburg, VA, USA

Copyright 2019 ARMA, American Rock Mechanics Association

This paper was prepared for presentation at the 53rd US Rock Mechanics/Geomechanics Symposium held in New York, NY, USA, 23–26 June 2019. This paper was selected for presentation at the symposium by an ARMA Technical Program Committee based on a technical and critical review of the paper by a minimum of two technical reviewers. The material, as presented, does not necessarily reflect any position of ARMA, its officers, or members. Electronic reproduction, distribution, or storage of any part of this paper for commercial purposes without the written consent of ARMA is prohibited. Permission to reproduce in print is restricted to an abstract of not more than 200 words; illustrations may not be copied. The abstract must contain conspicuous acknowledgement of where and by whom the paper was presented.

ABSTRACT: Hydraulic fracturing in shales is challenging because of the complicated stress status. The confining pressure imposed on a shale formation has a tremendous impact on the permeability of the rock. The correlation between confining pressure and rock permeability is complicated and might be nonlinear. Gas flow in low-permeability shales differs significantly from liquid flow because of the Klinkenberg effect, especially when the pore pressure is relatively low. The Klinkenberg effect results from gas molecule slip at the solid walls inside the nanopores, where the collision between gas molecules and solid surfaces is more frequent than the collision between gas molecules. This effect causes the increase of apparent permeability (i.e., the measured permeability). In this study, the simple effective stress law and the effective stress coefficient law were used to study the relationship between permeability and effective stress. In the simple effective stress law, the effective stress is calculated as the difference between confining pressure and pore pressure. The Klinkenberg coefficient and the effective mean pore radius can then be calculated. In the effective stress coefficient law, there is an effective stress coefficient (i.e., the Biot coefficient) which controls the influence of pore pressure on the effective stress. In this study, the effective stress coefficient was obtained by analyzing a large number of laboratory data measured under varying pore pressures and confining pressures. Specifically, the permeabilities of core samples extracted from four U.S. shale formations were measured using a pulse decay permeameter under varying combinations of confining and pore pressures. The samples were cored in the directions parallel to and perpendicular to the shale bedding planes, in order to test the role of bedding plane direction on the measured permeability. Laboratory results demonstrate that the permeabilities of all core samples fell in the range between 10^{-2} millidarcy (mD) and 10^{-4} mD. In the same formation, the permeabilities of the core samples in which the bedding planes were in the longitudinal direction were about one order of magnitude higher than the permeabilities of the core samples in which the bedding planes were in the transverse direction. Using the simple effective stress law, the Klinkenberg effect was observed, because the measured apparent permeability decreased with increasing pore pressure. Using the effective stress coefficient law, the effective stress coefficient was found around 0.5, which suggests that the pore pressure had a less influence on the effective stress compared to the confining pressure. Moreover, a multiphysical shale transport (MPST) model is built that accounts for fluid dynamics, geomechanics, and the Klinkenberg effect. The model fitting result is quite matched with PDP experimental results. These comprehensive laboratory experiments and model fitting demonstrate the role of confining pressure, Klinkenberg effect, and bedding plane direction on the gas flow in the nanoscale pore space in shales. These experimental data will be valuable in validating and calibrating pore- to core-scale numerical models of the flow and transport properties in shale formations.

Keywords: Apparent permeability, Klinkenberg effect, Pulse decay, Effective stress coefficient, MPST model.

1. INTRODUCTION

The complicated petrophysical properties and extremely low permeability of shale formations lead to extraordinary challenges to the development of unconventional hydrocarbon resources from these formations, such as shale oil and gas formations. Horizontal drilling associated with multi-stage hydraulic fracturing has become an effective technique to produce hydrocarbon resources from shales at an economically viable rate (Economides and Nolte, 2000; Gu and Mohanty, 2014; Chen et al., 2015; Hu et al., 2018). Fracture creation and propagation is an essential step in the process of hydraulic fracturing. In order to achieve this goal, the injection pressure should be higher than the minimum horizontal principal stress in the formation (Ye and Ghassemi, 2016). During hydrocarbon recovery, the decreased pore pressure leads to increased effective stress and fracture closure (Fan et al., 2017b, 2018). The effective stress variation has a significant impact on the petrophysical properties in the shale formation, especially the formation permeability. It is thus crucial to investigate the relationship between formation permeability and effective stress variation.

The investigation of the correlation between effective stress and rock permeability began with tight sandstones in the laboratory. Warpinski and Teufel (1992) performed

laboratory experiments to study the effective stress law in tight sandstone and chalk. They found that the effective stress coefficient (i.e., the Biot coefficient), α, in tight sandstone was close to unity for small stresses but contained uncertainties for larger stresses. The value of α varied with both effective stress and pore pressure. Zhang et al. (2000) set up laboratory experiments to test the dependence of permeability on loading conditions. It was found that the trend and magnitudes of permeability variations were controlled by the initial size of the fracture aperture, external load configuration, and rock deformation. The permeability changes appeared to be unpredictable when the rock deformation was in the inelastic stage. Chenevert and Sharma (1993) used laboratory-measured permeability and pore pressure data to characterize swelling pressure and spalling types of wellbore instability. Worthington (2004) quantified the dependence of permeability on mechanical stress through third-order polynomial formulation. The research outcome emphasized the importance of detailed field studies. Ojala and Fjær (2007) tested Castlegate sandstone cores under cyclic pore and confining pressure variations. Their results demonstrated that the effective stress coefficient under acoustic and elastic testing in the sandstone can be considerably different from unity. They also illustrated the hysteresis in petrophysical properties due to microfracture or frictional effects.

The Klinkenberg effect was proposed by Klinkenberg (1941) to explain the abnormal phenomenon of apparent permeability enhancement for gas flow in porous media. It has a significant impact on gas flow, especially in low permeability porous media such as shale reservoirs and tight coalbeds (Wu et al., 1998). The Klinkenberg effect is related to the Knudson (Kn) number, which is defined as $Kn = \lambda/d$, where λ is gas mean-free-path length (m) and d is pore diameter (m). When $Kn < 0.001$, gas flow is governed by the Navier-Stokes equation with a no-slip boundary condition on the pore walls. When $0.001 < Kn < 0.1$, gas flow is in the slip flow regime in which the non-continuum effect can be approximated by a velocity slip on the pore walls; the bulk gas flow can still be governed by the Navier-Stokes equation (Beskok and Karniadakis, 1999). The continuous increase in Kn leads to the transitional flow regime ($0.1 < Kn < 10$) and then the free molecular flow regime ($Kn > 10$), where the gas flow cannot be described by the Navier-Stokes equation any more (Dr. X. Yin, personal communication, 2018).

In a shale formation, when the nanopore diameter decreases or gas pressure decreases (lower gas pressure leads to a larger gas molecule mean-free-path length), the Kn number increases. In this scenario, the nanopore diameter can be comparable to or smaller than the mean-free-path length of gas molecules. As a consequence, gas molecules collide with the pore walls more frequently than with one another, leading to Knudsen diffusion that causes a slip-velocity boundary condition in the macroscopic Navier-Stokes flow model (Javadpour, 2009). The existence of the slip velocity on flow boundaries enhances the overall mass flux through the nanotube, which results in increased apparent permeability of the shale (Chen, 2016).

A series of analytical solutions was developed to characterize gas flow in tight porous media subjected to the Klinkenberg effect (Wu et al., 1998; Innocentini and Pandolfelli., 2001; Zhu et al., 2007; Hu et al., 2009; Hayek, 2015). Based on previous works in the literature, Firouzi et al. (2013) developed a non-equilibrium molecular dynamics model and then conducted pressure pulse decay experiments to compare the model predictions with laboratory measurements. They found that the laboratory measurements were about two orders of magnitude larger than the model predictions. Li et al. (2016) derived an analytical formula for gas effective permeability subjected to the Klinkenberg effect based on the microscale flow model and fractal capillary model. Their results demonstrated the physical meaning of the model parameters. In a complicated environment, such as polymer-water-oil flow in porous media, the Klinkenberg effect was found to be mitigated with the presence of an adsorption polymer layer (Blanchard et al., 2007). Moreover, the Klinkenberg coefficient cannot be treated as a constant in coalbeds due to the high compressibility and matrix swelling of coal (Wang et al., 2014). All the studies reviewed above confirm that the Klinkenberg effect exists in a wide range of subsurface flow and transport processes associated with geoenergy and geoenvironmental implications.

In this paper, we collected core samples from four U.S. shale formations, including Mancos, Eagle Ford, Barnett, and Marcellus, to investigate the correlations between apparent permeability, k_a, confining pressure, P_c, and effective stresses, P_e. We also tested core samples extracted in various directions; specifically, the cores extracted along the bedding planes included "PL" in the sample names, which means "parallel", whereas the cores extracted perpendicular to the bedding planes included "PD" in the sample names, which means "perpendicular". By doing this, the role of bedding plane direction on core permeability was unraveled. In this study, a core sample was tested using a pressure pulse decay permeameter (PDP), subjected to comprehensive combinations of pore pressures, P_p, and confining pressures, P_c. The gas used in the PDP is pure nitrogen. Measured permeability and pressure data were fitted using the simple effective stress law and the effective stress coefficient law. We then obtained the Klinkenberg coefficient, b, and the effective mean pore radius, r, using the simple effective stress law. Using the effective stress coefficient law, we derived the effective stress coefficient, χ, and then calculated P_e, which has a one-to-one correlation with measured

permeability, k. The value of $log\ (k)$ was plotted as a function of P_e to demonstrate the correlation between them. We then developed MPST model based on fluid dynamics, geomechanics, and the Klinkenberg effect to fit PDP experimental results. The fitting curves were then compared with experimental data. This comprehensive, laboratory experimental, and model fitting study advances the fundamental understanding of the role of confining pressure, pore pressure, Klinkenberg effect, and bedding plane direction on shale permeability. The research outcome has the potential to advance the scientific understanding of the relationship between geomechanical stress and flow and transport properties in a shale formation. Generated knowledge will be helpful in stress analysis and the optimization of hydraulic fracturing.

2. OVERVIEW OF THE EXPERIMENT/ANALYSIS WORKFLOW

This section aims to provide an overview of the experiment workflow. Details of experimental setup will be given in a later section. In this work, an experiment/analysis approach was developed to study the correlation between apparent permeability, k_a, and effective stress, P_e. First, a series of shale core samples, containing different bedding plane directions, were extracted from four U.S. shale formations. Second, a pressure pulse decay permeameter was used to measure core permeabilities with a wide range of various combinations of P_p and P_c. Third, the simple effective stress law was used to calculate the effective stress and to derive the Klinkenberg coefficient, b, and the mean pore radius, r, which are the petrophysical properties of core samples but vary when the effective stress varies. Fourth, the experimental laboratory data were fitted to the model based on the effective stress coefficient law, and the effective stress coefficient, χ, was obtained for each core sample. Finally, MPST model was derived based on fluid dynamics, geomechanics, and the Klinkenberg effect. The model curves were compared with experimental curves.

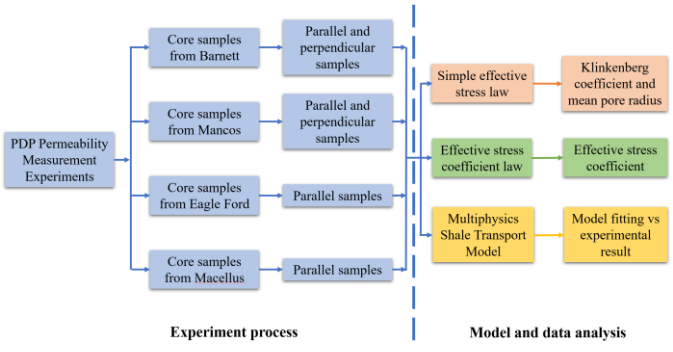

Figure 1. An experiment/analysis workflow for the assessment of the correlation between apparent permeability, confining pressure, effective stress, and MPST model.

In this study, based on the simple effective stress law, we selected 500 psi, 1000 psi, and 1500 psi as the values of the effective stress, P_e, for each core sample. For each effective stress value, eight pore pressure values (100 psi, 300 psi, 500 psi, 700 psi, 900 psi, 1100 psi, 1300 psi, and 1500 psi) were tested using PDP, and the confining pressures were calculated as the sum of the pore pressures and the particular effective stress based on the simple effective stress law. Therefore, we conducted in total 24 PDP experiments for a single shale core sample which was subjected to different combinations of P_e and P_p. The experimental results of the cores containing different bedding plane directions were compared with each other to unravel the role of bedding plane direction on the core permeability. The same experimental data were then used to fit the effective stress coefficient law and consequently to find the effective stress coefficient, χ.

3. MODELS AND EXPERIMENTAL EQUIPMENT

3.1. *Simple effective stress law and Klinkenberg equation*

It is the Klinkenberg effect that leads to the difference between apparent permeability and absolute permeability, especially under low pore pressure. Using the simple effective stress law, the effective stress, P_e, is calculated as $P_e = P_c - P_p$. In order to quantify the Klinkenberg effect, the Klinkenberg coefficient (Klinkenberg, 1941) was used to describe the role of pore pressure on the apparent permeability. The Klinkenberg coefficient depends on the petrophysical properties of the rock, and is included in the Klinkenberg equation written as follows:

$$\frac{k_a}{k} = 1 + \frac{b}{P_p} \tag{1}$$

where k_a is the apparent permeability (m^2), P_p is the pore pressure (Pa), k is the absolute permeability of the porous medium (m^2), and b is the Klinkenberg coefficient which is expressed as (Chen, 2016)

$$b = \frac{\mu}{r}\left(\frac{2}{\alpha} - 1\right)\sqrt{\frac{8\pi RT}{M}} + \frac{16\mu}{3r}\sqrt{\frac{8RT}{\pi M}} \tag{2}$$

where μ is dynamic viscosity (Pa·s); α is the tangential momentum accommodation coefficient with a value from 0 to 1; R is the gas constant and equal to 8.314 J/mol/K; T is the absolute temperature (K); M is molar mass (kg/mol); and r is the effective pore radius (m). Using Equation 2, one can calculate r as:

$$r = \frac{\mu}{b}\left(\frac{2}{\alpha} - 1\right)\sqrt{\frac{8\pi RT}{M}} + \frac{16\mu}{3b}\sqrt{\frac{8RT}{\pi M}} \tag{3}$$

3.2. *Effective stress coefficient law*

The effective stress coefficient law assumes that P_e is not simply the difference between confining pressure and pore pressure (P_c - P_p) but is written as (Bernabe, 1986):

$$P_e = P_c - \chi P_p \quad (4)$$

where P_e is effective stress (Pa), P_c is confining pressure (Pa), P_p is pore pressure (Pa), and χ is the effective stress coefficient, whose value depends on the specific rock mineral composition. Equation 4 suggests that the effective stress has different sensitivities to the confining pressure and pore pressure if the value of χ is not equal to one. The basic assumption of the effective stress coefficient law is that the permeability depends on the effective stress, which controls the pore geometry and pore size in the rock. If the effective stress stays the same, then the permeability is a constant.

Because P_e is a function of P_p and P_c, k can be written as a function of these two variables:

$$k = k(P_c, P_p) \quad (5)$$

Because the permeability of natural geologic formations in general follows a lognormal distribution (Chen and Zeng, 2015), we use *log(k)* as an indicator of the formation permeability and then have:

$$log\ (k) = log\ (k)(P_c, P_p) \quad (6)$$

Based on Equation 6, one obtains the differential of *log(k)*:

$$dlog(k) = \left(\frac{\partial log(k)}{\partial P_c}\right) dP_c + \left(\frac{\partial log(k)}{\partial P_p}\right) dP_p \quad (7)$$

One also has the following equation based on Equation 4:

$$dP_e = dP_c - \chi dP_p \quad (8)$$

When the effective stress stays constant, both d*log(k)* and dP_e are zero. Therefore, one obtains:

$$\left(\frac{\partial log(k)}{\partial P_c}\right) dP_c + \left(\frac{\partial log(k)}{\partial P_p}\right) dP_p = 0 \quad (9)$$

and

$$dP_c - \chi dP_p = 0 \quad (10)$$

Using Equations 9 and 10, one obtains:

$$\chi = -\left(\frac{\partial log(k)}{\partial P_p}\right) / \left(\frac{\partial log(k)}{\partial P_c}\right) \quad (11)$$

3.3. Pressure pulse decay experiment

The pressure pulse decay permeameter (PDP) equipment is convenient, dynamic approach to measuring the permeability of tight rocks. Jones (1997) developed the basic measurement principle of PDP. He found that the measurement range of PDP is from 0.1 mD to 0.01 microdarcy (μD). As opposed to traditional permeability measurement methods, which use flow parameters in the steady state and are based on Darcy's law, the PDP method uses transient flow parameters, which significantly accelerates the measurement process and consequently is ideal for low-permeability rocks. **Figure 2** is a schematic plot of the PDP setup. The flow rate measurement is not required but can be calculated from the known volumes of the reservoirs, fluid compressibility, and the rate of change of gas pressures (Hseih et al., 1981; Bourbie and Walls, 1982).

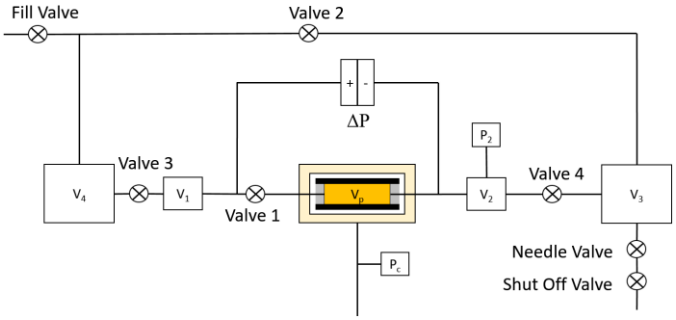

Figure 1. Schematic PDP equipment setup, which consists of an upstream test gas reservoir having a volume of V_1, a high-pressure core holder with the pore volume of V_p, a downstream gas reservoir having a volume of V_2, a differential pressure transducer to continuously measure the pressure difference (ΔP) between the upstream and downstream reservoirs, and a second pressure transducer to measure the downstream reservoir pressure, P_2. This picture is from Core Lab PDP-200 operations manual.

Figure 3 demonstrates the shale core samples collected from four different U.S. shale formations, including the Eagle Ford, Marcellus, Mancos, and Barnett formations. The pore pressure, P_p, throughout the core sample is uniform in the initial stage. When t = 0, a gas pressure slightly higher than the initial pore pressure is imposed at the upstream end of the core sample at. During the process of gas flow into the core sample from the upstream reservoir, the gas pressure in the upstream reservoir declines. When the pressure pulse propagates through the core sample and then reaches the downstream end, the gas pressure in the downstream reservoir increases. After a certain period of time, the differential pressure between the upstream and downstream reservoirs approaches zero. The decay rate of the differential pressure is proportional to the permeability of the core sample. Dicker and Smits (1988) developed the general analytical solution of the differential pressure as a function of time. Chen and Stagg (1984) and Haskett et al. (1988) also made contributions to analytical solutions.

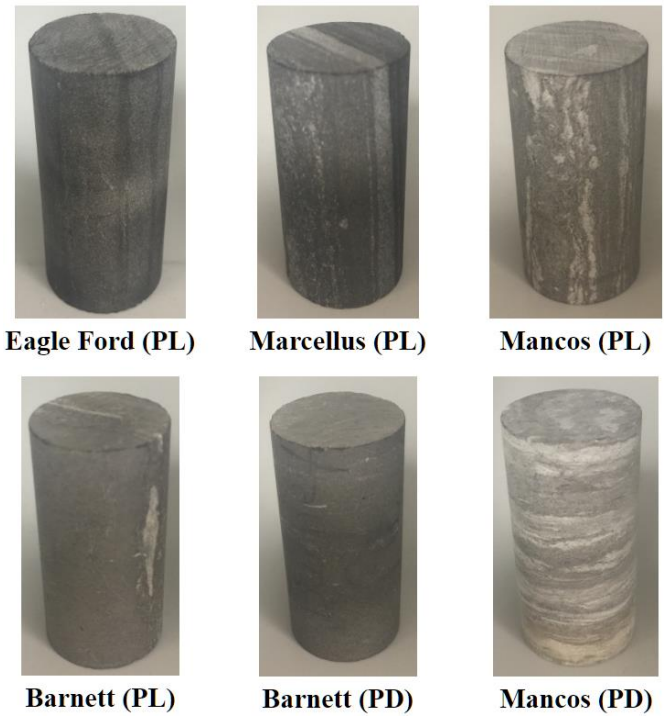

Figure 2. Core samples used in the PDP tests. The core samples were extracted from four U.S. shale formations, including the Eagle Ford, Marcellus, Mancos, and Barnett formations. "PL" denotes that the core axis direction is parallel to the bedding plane direction, whereas "PD" indicates that the core axis direction is perpendicular to the bedding plane direction.

4. MULTIPHYSICS SHALE TRANSPORT MODEL

As illustrated by the permeability result of PDP experiment and CT images (Chen, 2016), the shale rocks don't have homogeneous pore size and mineral compositions, thus leading the heterogeneous compressibility in the shale rocks. Recent studies demonstrated that the pore volume in the inorganic matrix is larger than that in the intrakerogen (Chen et al., 2013; Chen et al., 2016). Based on the investigations above, a MPST model is built that accounts for fluid dynamics, geomechanics, and the Klinkenberg effect. **Figure 4** illustrates the schematic MPST model. Pore pressure, P_p, and effective stress, P_e, are the two independent variables of this model, and the model apparent permeability, $\bar{k}$, is the model output. This model contains two parts: kerogen and inorganic matrix, which have their own permeability, compressibility, and pore width. The model is surrounded by compressive stress.

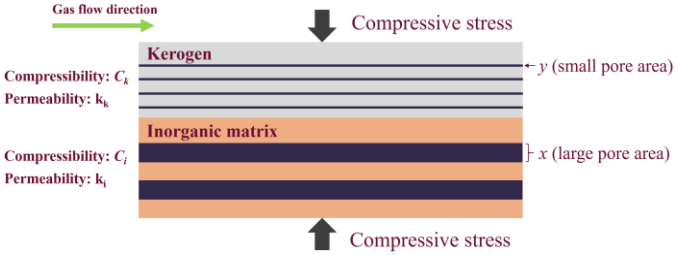

Figure 3. Schematic multiphysics shale transport model. This model contains two parts: kerogen and inorganic matrix. They both have their own permeability and compressibility. The pores in the kerogen are small pores which have the width of y. The pores in the inorganic matrix are large pores which have the width of x. The small pore and large pore have a number ratio N. The model is surrounded by compressive stress.

The absolute permeability of kerogen and inorganic matrix can be obtained by $k = d^2/12$ where d is pore diameter. Combined with Equation 1, one can obtain

$$k_i = \frac{x^2}{12}\left(1 + \frac{b(x)}{P}\right)$$
$$k_k = \frac{y^2}{12}\left(1 + \frac{b(y)}{P}\right) \quad (12)$$

where b(a) and b(b) mean Klinkenberg coefficient b is the function of large pore area a and small pore area b, respectively. Meanwhile, the output of this model, model apparent permeability $\bar{k}$, can be calculated using Darcy's law:

$$\bar{k} = \frac{\bar{u}\cdot\mu}{\nabla P} = \frac{(Q_i + Q_k)\mu}{A\cdot\nabla P} \quad (13)$$

where A is model total area which can be expressed as $A = \frac{x+N\cdot y}{\phi}$. $\bar{u}$ is average flow velocity which can be calculated as $\bar{u} = \frac{Q_i+Q_k}{A}$. N is number ratio of small pore and large pore in the model. Besides, the flow rate of shale gas in the kerogen Q_k and inorganic matrix Q_i can be calculated respectively with Equation 12 as follows:

$$Q_i = u_i\cdot x = \frac{k_i}{\mu}\cdot\nabla P\cdot x = \frac{x^3}{12}\cdot\frac{\nabla P}{\mu}\left(1+\frac{b(x)}{P}\right)$$
$$Q_k = Nu_k\cdot y = \frac{k_k}{\mu}\cdot\nabla P\cdot y = \frac{Ny^3}{12}\cdot\frac{\nabla P}{\mu}\left(1+\frac{b(y)}{P}\right) \quad (14)$$

The absolute permeability calculation formula of MPST model is $k = d^2/12$ instead of $k = r^2/8$ where d is pore diameter and r is pore radius. Thus, one can re-write Equation 2 for the kerogen and inorganic matrix as

$$b(x) = \frac{\mu}{x}\left(\frac{2}{\alpha}-1\right)\sqrt{\frac{8\pi RT}{M}} + \frac{2\mu}{x}\sqrt{\frac{8RT}{\pi M}}$$
$$b(y) = \frac{\mu}{y}\left(\frac{2}{\alpha}-1\right)\sqrt{\frac{8\pi RT}{M}} + \frac{2\mu}{y}\sqrt{\frac{8RT}{\pi M}} \quad (15)$$

Pore area x and y in Equation 15 depend on effective stress and can be obtained as

$$x = x_0[1 - C_i\Delta P_e]$$
$$y = y_0[1 - C_k\Delta P_e] \quad (16)$$

where x_0 and y_0 are reference area of x and y, C_i and C_k is the compressibility of inorganic matrix and kerogen.

The porosity of MPST model can be calculated with Equation 16 as

$$\phi = \frac{x + Ny}{x + Ny + S} = \frac{x_0[1 - C_i\Delta P_e] + Ny_0[1 - C_k\Delta P_e]}{x_0[1 - C_i\Delta P_e] + Ny_0[1 - C_k\Delta P_e] + S} \quad (17)$$

Substituting Equations 14, 15, 16, and 17 into Equation 13, one can re-write Equation 13 as follows:

$$k = \frac{x_0[1 - C_i\Delta P_e] + Ny_0[1 - C_k\Delta P_e]}{x_0[1 - C_i\Delta P_e] + Ny_0[1 - C_k\Delta P_e] + S} \cdot \frac{x_0^3(1 - C_i\Delta P_e)^3\left[1 + \frac{\mu\left(\frac{2}{\alpha} - 1\right)\sqrt{\frac{8\pi RT}{M}} + 2\mu\sqrt{\frac{8RT}{\pi M}}}{x_0(1 - C_i\Delta P_e)P}\right] + y_0^3(1 - C_k\Delta P_e)^3\left[1 + \frac{\mu\left(\frac{2}{\alpha} - 1\right)\sqrt{\frac{8\pi RT}{M}} + 2\mu\sqrt{\frac{8RT}{\pi M}}}{y_0(1 - C_k\Delta P_e)P}\right]}{12[x_0(1 - C_i\Delta P_e) + Ny_0(1 - C_k\Delta P_e)]} \quad (18)$$

5. RESULTS AND DISCUSSION

Figure 5 illustrates PDP-measured apparent permeability as a function of pore pressure under different effective stresses in the cores of Mancos PL, Mancos PD, Barnett PL, Barnett PD, Eagle Ford PL, and Marcellus PL. All the six groups of PDP tests demonstrated that the apparent permeability decreased with increasing pore pressure when the effective stress was constant based on the simple effective stress law. The sample of Mancos PL had the highest average permeability across all pore pressures, whereas the sample of Mancos PD had the lowest average permeability. Because high pore pressure can mitigate the Klinkenberg effect (Vermylen, 2011), in this study, we considered the average value of the apparent permeabilities at the pore pressures of 1300 psi and 1500 psi as the absolute permeability of the core. Specifically, Soeder (1988) used laboratory tests to measure permeability under varying pore pressures for cores extracted from the Marcellus shale. He found that when the pore pressure was higher than 500 psi, permeability change was smaller than 15%. Therefore, the apparent permeabilities measured under 1300 and 1500 psi were very close to the absolute permeability. It was found that the absolute permeabilities of all core samples ranged from 10^{-4} m D to 10^{-2} mD. In addition, it was noticed that in the same shale formation the permeabilities in the cores where the bedding planes were parallel to the core axis were approximately one order of magnitude higher than those in the cores where the bedding planes were perpendicular to the core axis. This is because the pore spaces between bedding planes have higher connectivity and thus provide higher gas flow conductivity, leading to higher permeability if the sample is cored in this direction. The effective stress is a critical parameter which has a great impact on the PDP-measured apparent permeability. Under high effective stress (1500 psi), the apparent permeability did not change noticeably when the pore pressure increased. This was because that for most core samples there existed connected pore networks having various spatial scales. The relatively small pore networks were more sensitive to effective stress, and they shut off when the effective stress increased, leaving relatively large pore networks open, which were relatively insensitive to the Klinkenberg effect and thus had relatively smaller Klinkenberg coefficients. The relatively high effective stress (1500 psi) effectively reduced the sizes of the connected gas flow channels contained in the organic-rich materials, leading to enhanced Klinkenberg coefficient, b, and consequently higher apparent permeabilities. When the effective stress was 500 psi, the apparent permeabilities decreased noticeably with increasing pore pressure, which suggests that the Klinkenberg effect was significant under the relatively low effective stress because all relatively small pore networks stayed open.

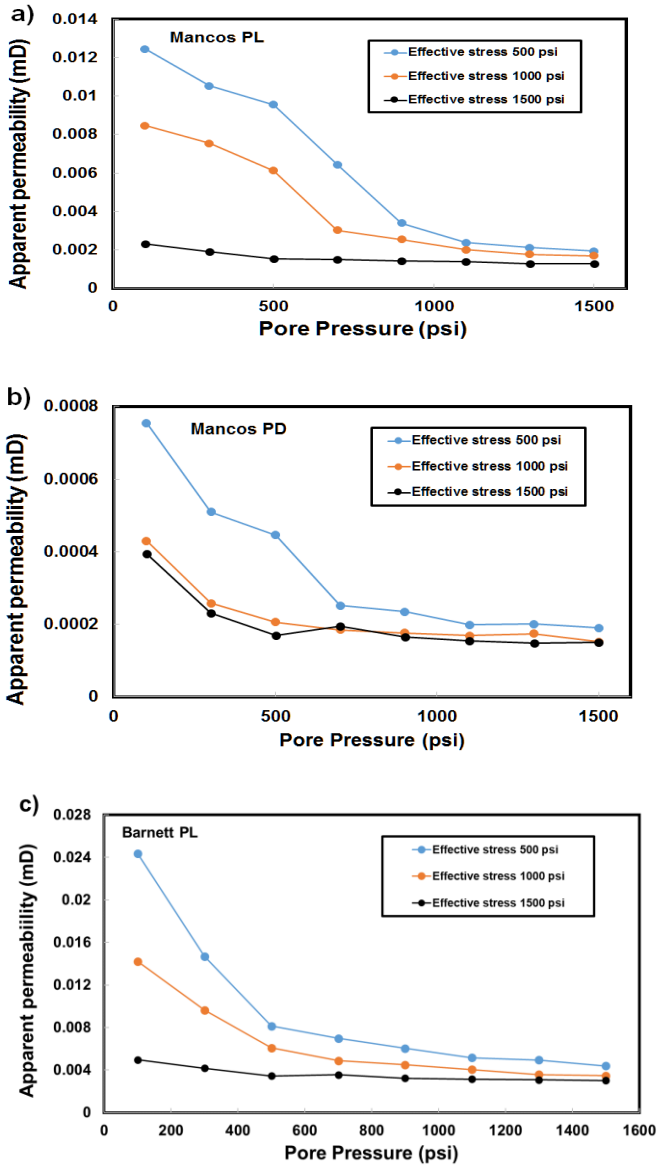

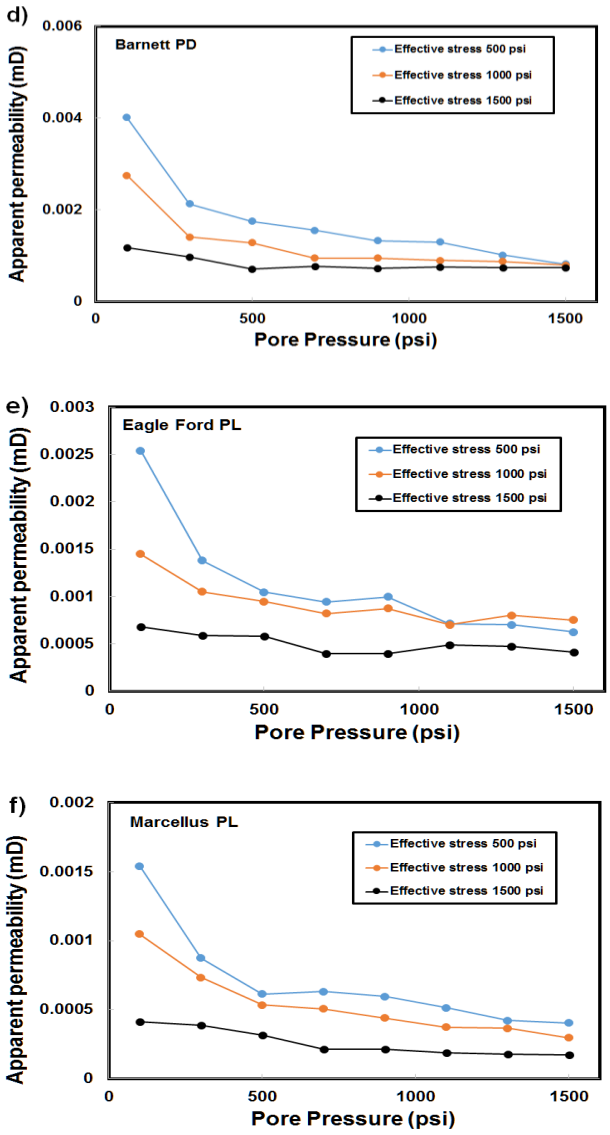

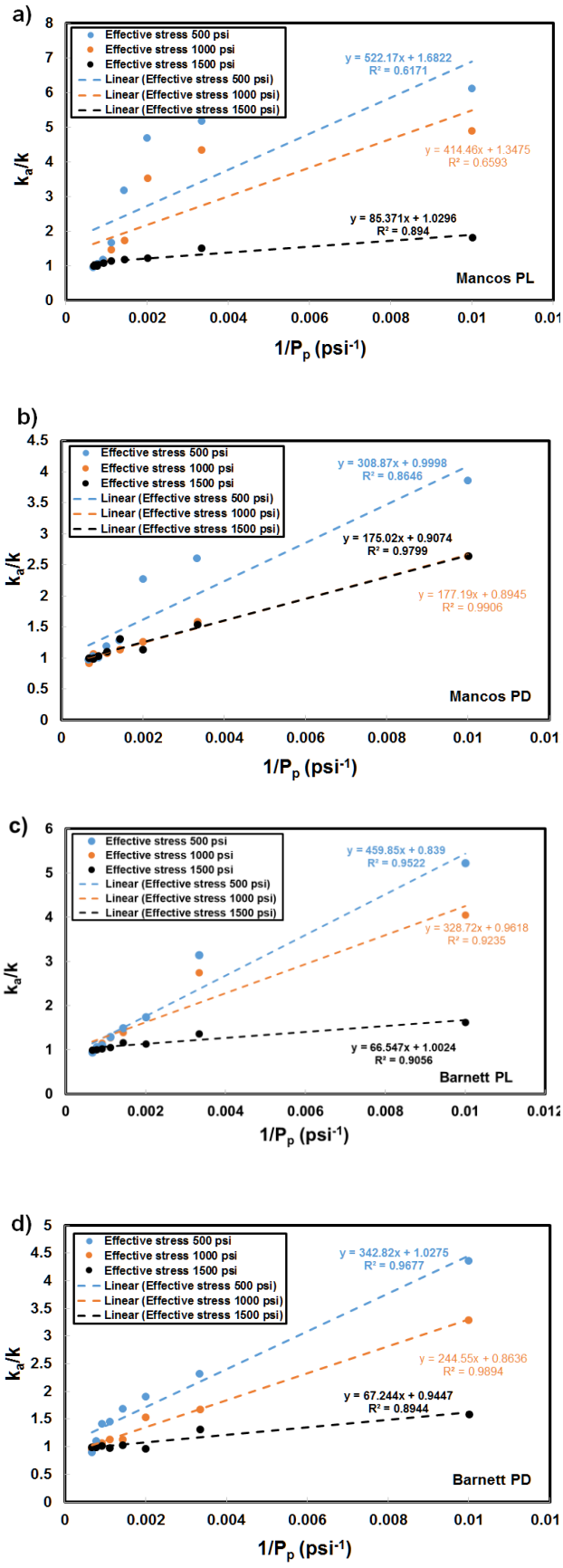

Figure 4. Apparent permeability as a function of pore pressure under different effective stresses in the core of a) Mancos PL, b) Mancos PD, c) Barnett PL, d) Barnett PD, e) Eagle Ford PL, and f) Marcellus PL.

Figure 6 illustrates k_a/k as a function of $1/P_p$, as well as the linear equation fitting, in the core samples of Mancos PL, Mancos PD, Barnett PL, Barnett PD, Eagle Ford PL, and Marcellus PL. Based on Equation 1, the y-intercept of the linear equation is 1, and the slope is equal to the Klinkenberg coefficient, *b*, in the unit of psi. The variation of the value of *b*, as a function of the effective stress across the six shale core samples, was consistent with the description and explanation in Figure 5. It was also noticed that the values of *b*, most of which fell into the range between 100 psi and 400 psi, were close to what were found in the literature based on laboratory (Soeder, 1988) and analytical (Chen, 2016) methods.

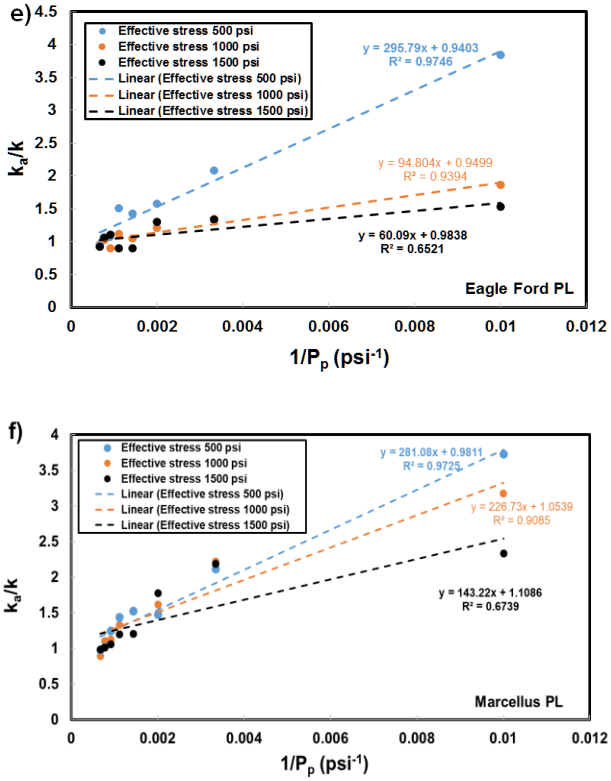

Figure 5. k_a/k as a function of $1/P_p$, as well as the linear equation fitting, in the core samples of a) Mancos PL, b) Mancos PD, c) Barnett PL, d) Barnett PD, e) Eagle Ford PL, and f) Marcellus PL. Based on Equation 1, the y-intercept of the linear equation is 1 and the slope is equal to the Klinkenberg coefficient, b.

We then used the data fitting method, which was originally developed by Bernabe (1986) and then improved by Kwon et al. (2001), to find the effective stress coefficient (i.e., the Biot coefficient), χ, in the effective coefficient law (i.e., Equation 4). **Figure 7** illustrates *log(k)* as a function of the confining pressure, P_c, under varying pore pressures. The slope of the fitted straight lines was equal to $\partial log(k)/\partial P_c$. Based on the method of Kwon et al. (2001), the value of $\partial log(k)/\partial P_c$ in the same core sample should be constant and independent of the selected pore pressure, which is confirmed in Figure 7. Thus, in this study we used the data measured under the pore pressure of 1500 psi to fit $\partial log(k)/\partial P_c$. It should be noted that in the same core sample the slopes of the straight lines fitted under the other pore pressures were close to that for the pore pressure of 1500 psi. Figure 7 demonstrates that the value of $\partial \log(k)/\partial P_c$ ranges from 4×10^{-5} to 4×10^{-4}.

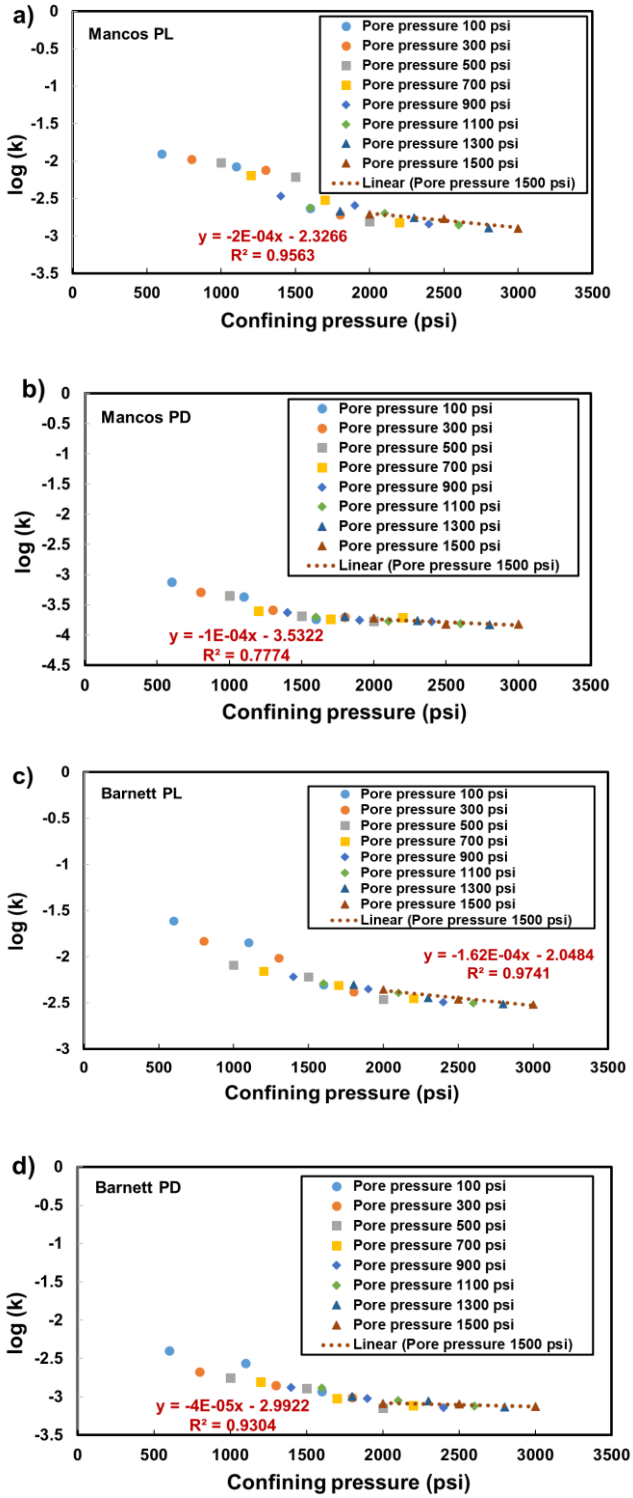

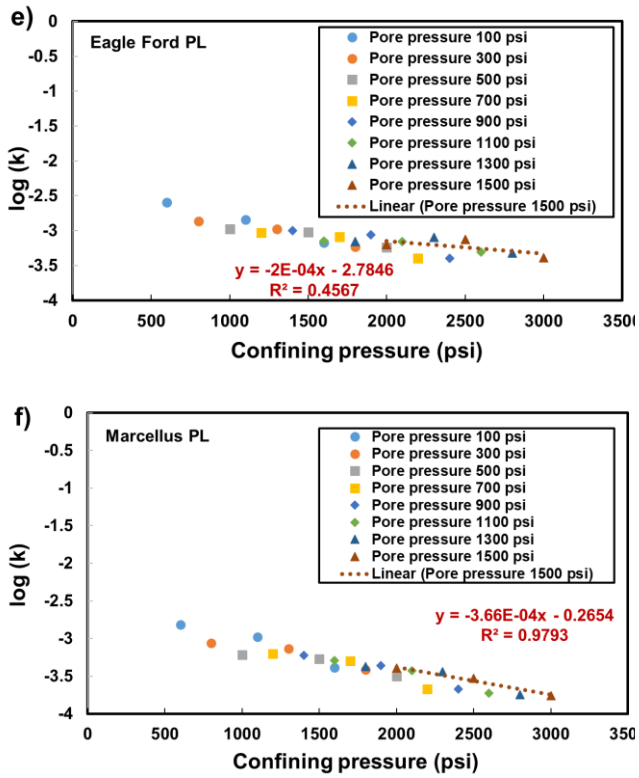

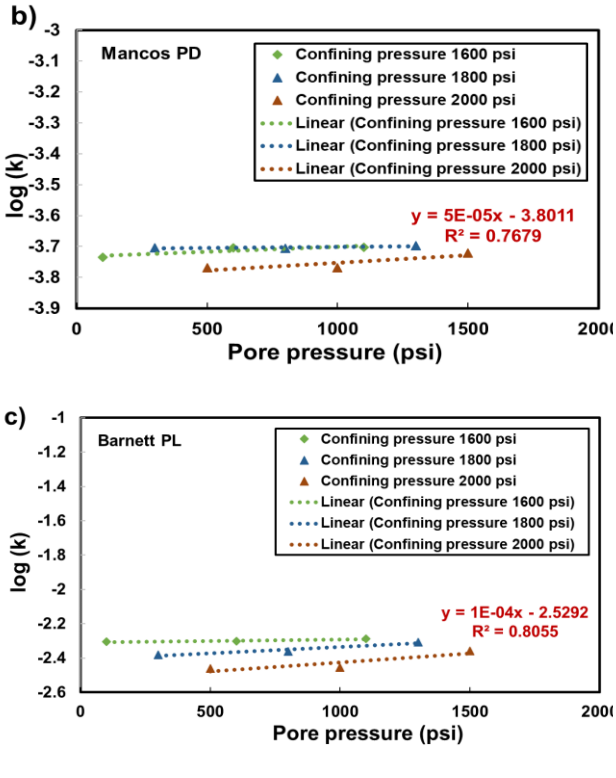

Figure 6. The value of log (k) as a function of the confining pressure, Pc, under varying pore pressures in the formations of a) Mancos PL, b) Mancos PD, c) Barnett PL, d) Barnett PD, e) Eagle Ford PL, and f) Marcellus PL.

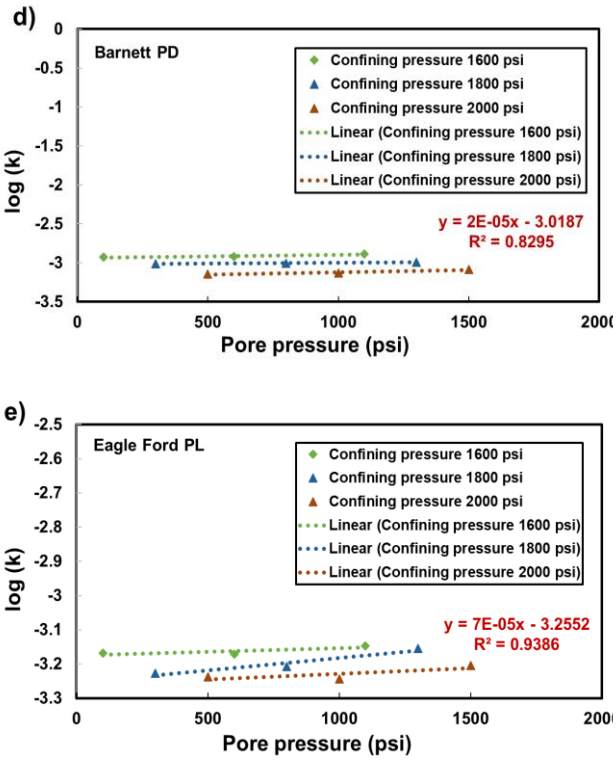

Figure 8 illustrates *log(k)* as a function of the pore pressure, P_p, under varying confining pressures. The slope of the fitted straight lines was equal to $\partial log(k)/\partial P_p$. Based on the method of Kwon et al. (2001), the value of $\partial log(k)/\partial P_p$ in the same core sample should be constant and independent of the selected confining pressure, which is confirmed in Figure 8. Thus, in this study we used the data measured under the confining pressure of 2000 psi to fit $\partial log(k)/\partial P_p$. It should be noted that in the same core sample the slopes of the straight lines fitted under the other confining pressures were close to that for the confining pressure of 2000 psi. Figure 8 demonstrates that the value of $\partial log(k)/\partial P_p$ ranges from 2×10^{-5} to 1×10^{-4}.

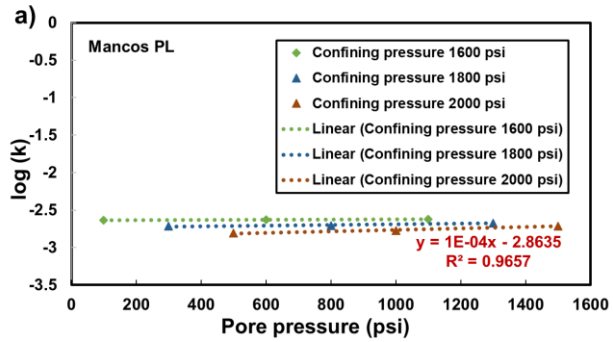

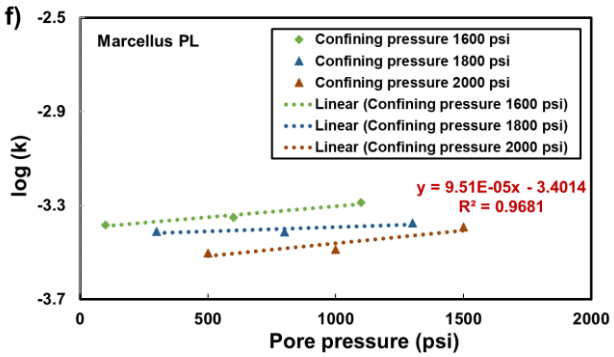

Figure 7. The value of log (k) as a function of pore pressure in the formations of a) Mancos PL, b) Mancos PD, c) Barnett PL, d) Barnett PD, e) Eagle Ford PL, and f) Marcellus PL.

Based on the results from Figures 7 and 8, we calculated the values of χ in the six shale formations using Equation 11. Specifically, the values of χ in t he four core samples were 0.50, 0.50, 0.62, 0.50, 0.35 and 0.26, respectively. **Figure 9** illustrates PDP-measured apparent permeability as a function of the effective stress calculated based on χ in the six formations. The result demonstrates that in general the PDP-measured apparent permeability decreases with the increase of the effective stress calculated based on χ.

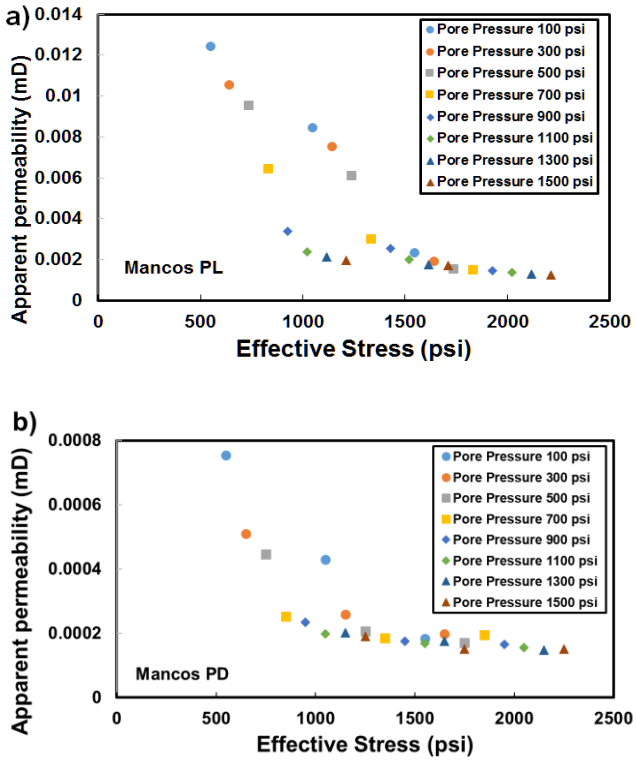

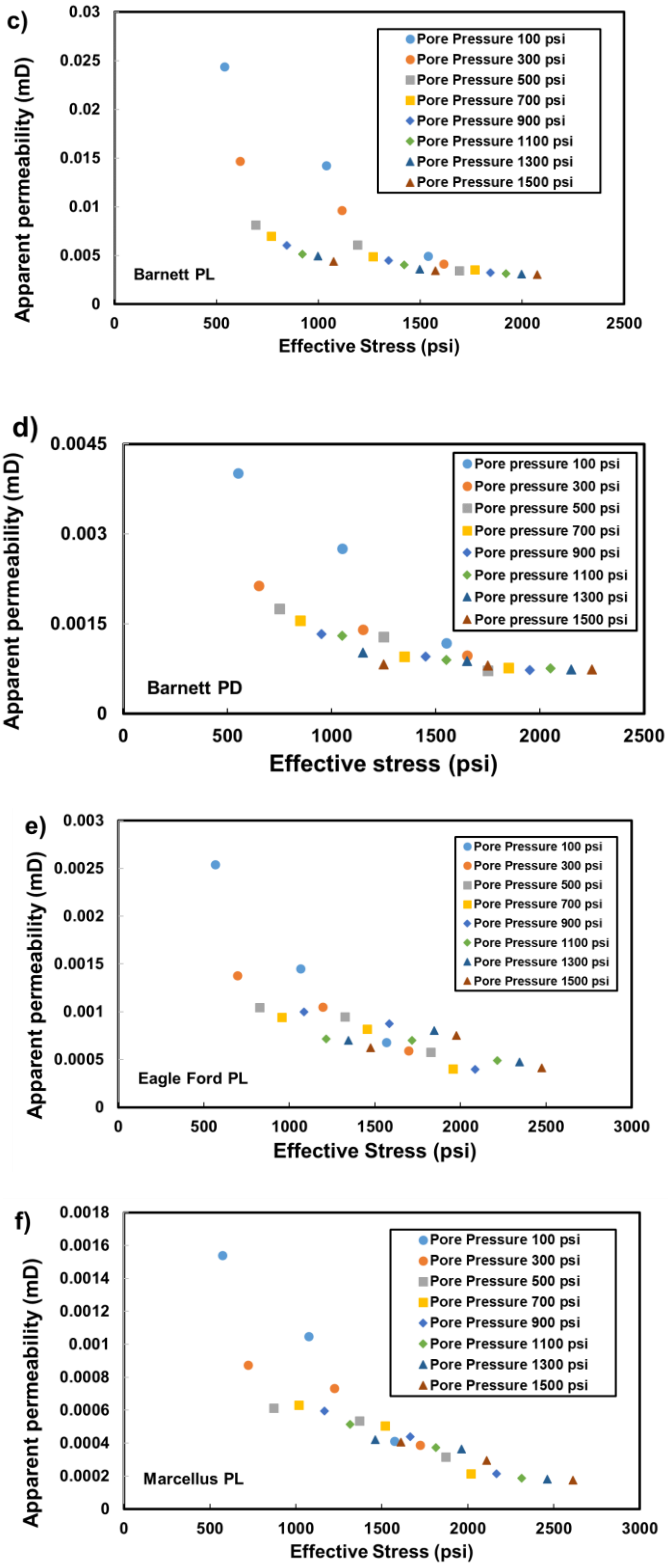

Figure 8. PDP-measured apparent permeability as a function of the effective stress calculated based on χ in a) Mancos PL, b) Mancos PD, c) Barnett PL, d) Barnett PD, e) Eagle Ford PL, and f) Marcellus PL.

Figure 10 illustrates the fitting apparent permeability curves of six core samples from MPST model. In MPST

model, pore pressure, P_p, and effective stress, P_e, are the two independent variables of this model, and the model apparent permeability, $\bar{k}$, is the model output. The x-axis unit of fitting curves is pore pressure and y-axis unit is apparent permeability, which are the same as Figure 5. MPST model takes into account gas transport in the organic and inorganic pores, compression of both kerogen (organic matters) and inorganic matrix under stress, and the Klinkenberg effect. Figure 10 demonstrates the trends of apparent permeability variation as functions of P_p and P_e. By fitting the PDP laboratory data, we found that the location of the permeability curve (up and down) is controlled primarily by the pore area, x and y, whereas the shape of the curve (curvature) is controlled primarily by kerogen compressibility, C_k. Besides, solid area S controls the magnitude of the curves. Future model improvement is needed in the high-pore-pressure range. The workflow of model fitting is as follows

Step 1. Adjust x_0 and y_0, the location of curves (up and down) is controlled by x_0 and y_0.

Step 2. Adjust C_i, the maximum value of curve is controlled by C_i. Besides, the shape of low P_e curves is also influenced by C_i.

Step 3. Adjust C_k, C_k controls the spacing of each curve, as well as their curvatures.

Step 4. Adjust S, the magnitude of y-axis is controlled by S but the shape of curves won't be influence (just change the value of y-axis).

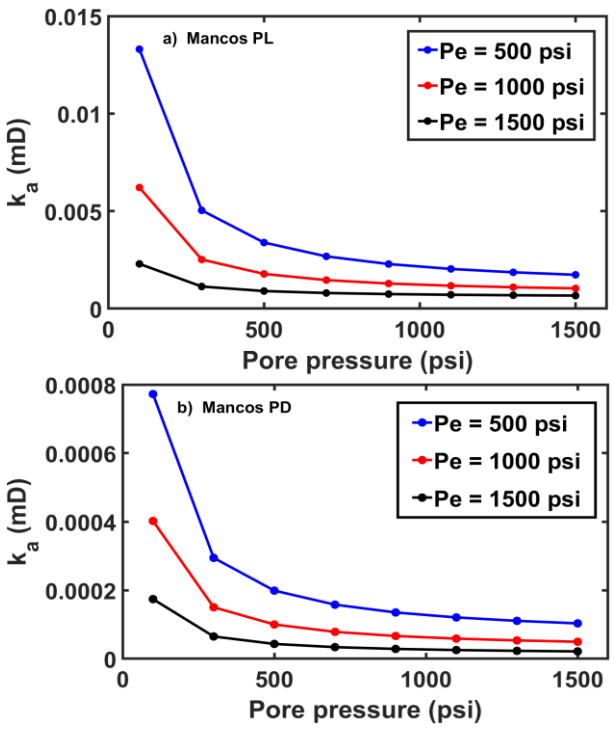

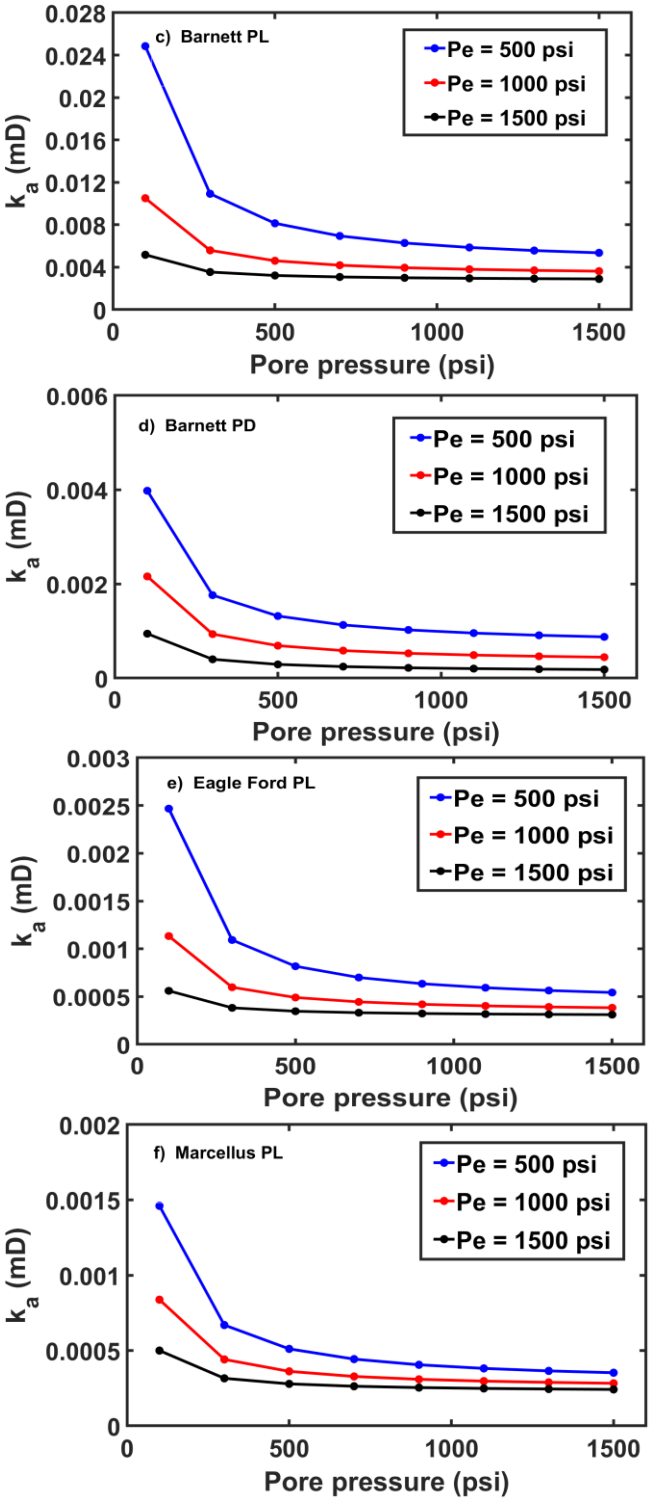

Figure 9. MPST model apparent permeability as a function of pore pressure under different effective stresses in the core of a) Mancos PL, b) Mancos PD, c) Barnett PL, d) Barnett PD, e) Eagle Ford PL, and f) Marcellus PL.

6. CONCLUSIONS

In this study, comprehensive core analyses based on the PDP method were conducted to investigate the relationships between apparent permeability, pore pressure, and confining pressure. The influence of the

Klinkenberg effect, as well as the direction of bedding planes, on the PDP-measured apparent permeability was also studied. Based on large volumes of data analytics, the effective stress coefficient (i.e., the Biot coefficient) was determined. The laboratory results indicate that in the same shale formation the permeabilities of the cores where the bedding planes were parallel to the core axis were approximately one order of magnitude higher than those in the cores where the bedding planes were perpendicular to the core axis.

Under high effective stress, the apparent permeability did not change noticeably when the pore pressure increased. This was because that for most core samples there existed connected pore networks having heterogeneous spatial scales. The relatively small pore networks were more sensitive to effective stress and they shut off when the effective stress increased, leaving relatively large pore networks open, which were relatively insensitive to the Klinkenberg effect and thus had relatively small Klinkenberg coefficients. The relatively high effective stress effectively reduced the sizes of the connected gas flow channels contained in the organic-rich materials, leading to enhanced Klinkenberg coefficient and consequently higher apparent permeabilities.

MPST model takes into account gas transport in the organic and inorganic pores, compression of both kerogen (organic matters) and inorganic matrix under stress, and the Klinkenberg effect. Pore pressure, P_p, and effective stress, P_e, are the two independent variables of this model, and the model apparent permeability, $\bar{k}$, is the model output. Model fitting curves demonstrates the trends of apparent permeability variation as functions of P_p and P_e. By fitting the PDP laboratory data, we found that the location of the permeability curve (up and down) is controlled primarily by the pore area, *x* and *y*, whereas the shape of the curve (curvature) is controlled primarily by kerogen compressibility, C_k. Besides, solid area *S* controls the magnitude of the curves. Future model improvement is needed in the high-pore-pressure range.

This study advances the fundamental understanding of the role of confining pressure, pore pressure, and bedding plane direction on the apparent permeability of shales. The research outcome has the potential to benefit the optimization of engineering design in hydraulic fracturing. The laboratory experiments provide insight into the Klinkenberg effect and its role on the apparent permeability under varying confining pressures in different U.S. formations.

ACKNOWLEDGEMENT

The authors are thankful to the funding support of the Junior Faculty Award from Virginia Tech's Institute for Critical Technology and Applied Science, as well as the financial assistance provided by the U.S. Department of Energy through the National Energy Technology Laboratory's Program under Contract No. DE-FE0031576. The authors are also grateful to Dr. Xiaolong Yin, Dr. Yongqiang Tang, and Ms. Ye Zang for helpful discussion.

REFERENCE

Bernabe, Y. 1986. The effective pressure law for permeability in Chelmsford granite and Barre granite. In International Journal of Rock Mechanics and Mining Sciences & Geomechanics Abstracts (Vol. 23, No. 3, pp. 267-275). Pergamon.

Beskok, A., and Karniadakis, G. E. A model for flows in channels, pipes, and ducts at micro and nano scales. *Microscale Thermophysical Engineering* 3:43-77, 1999.

Blanchard, V., Lasseux, D., Bertin, H. J., Pichery, T. R., Chauveteau, G. A., Tabary, R., & Zaitoun, A. 2007. Gas/water flow in porous media in the presence of adsorbed polymer: Experimental study on non-darcy effects. *SPE Reservoir Evaluation & Engineering*, 10(04), 423-431.

Bourbie, T., & Walls, J. 1982. Pulse decay permeability: analytical solution and experimental test. *Society of Petroleum Engineers Journal*, 22(05), 719-721.

Chen, C. 2016. Multiscale imaging, modeling, and principal component analysis of gas transport in shale reservoirs. *Fuel*, 182, 761-770.

Chen, C., Hu, D., Westacott, D., & Loveless, D. (2013). Nanometer-scale characterization of microscopic pores in shale kerogen by image analysis and pore-scale modeling. *Geochemistry, Geophysics, Geosystems*, 14(10), 4066-4075.

Chen, C., Martysevich, V., O'Connell, P. et al. 2015. Temporal Evolution of the Geometrical and Transport Properties of a Fracture/Proppant System under Increasing Effective Stress. SPE J. 20 (3): 527–535. SPE-171572-PA. https://doi.org/10.2118/171572-PA.

Chen, C., and L. Zeng (2015), Using the level set method to study the effects of heterogeneity and anisotropy on hyporheic exchange, Water Resour. Res., 51, 3617–3634, doi:10.1002/2014WR016444.

Chen, C., Wang, Z., Majeti, D., Vrvilo, N., Warburton, T., Sarkar, V., & Li, G. (2016). Optimization of lattice Boltzmann simulation with graphics-processing-unit parallel computing and the application in reservoir characterization. *SPE Journal*, 21(04), 1-425.

Chen, T., & Stagg, P. W. 1984. Semilog analysis of the pulse-decay technique of permeability measurement. *Society of Petroleum Engineers Journal*, 24(06), 639-642.

Chenevert, M. E., & Sharma, A. K. 1993. Permeability and effective pore pressure of shales. *SPE Drilling & completion*, 8(01), 28-34.

Dicker, A. I., & Smits, R. M. 1988. A practical approach for determining permeability from laboratory pressure-pulse decay

measurements. In International meeting on petroleum engineering. *Society of Petroleum Engineers*.

Economides M, Nolte K. *Reservoir Stimulation*. 2000.3rd edition: John Wiley and Sons.

Fan, M., Han, Y., McClure, J., and Chen, C. 2017b. Hydraulic Fracture Conductivity as a Function of Proppant Concentration under Various Effective Stresses: From Partial Monolayer to Multilayer Proppants. *Unconventional Resources Technology Conference*. doi:10.15530/URTEC-2017-2693347.

Fan, M., McClure, J., Han, Y., Li, Z., and Chen, C. 2018. Interaction Between Proppant Compaction and Single-/Multiphase Flows in a Hydraulic Fracture. SPE-189985-PA. SPE J. doi:10.2118/189985-PA.

Firouzi, M., Alnoaimi, K., Kovscek, A., & Wilcox, J. 2014. Klinkenberg effect on predicting and measuring helium permeability in gas shales. *International Journal of Coal Geology*, 123, 62-68.

Gu M, Mohanty KK. 2014. Effect of foam quality on effectiveness of hydraulic fracturing in shales. *Int J Rock Mech Min*. 70: 273-85.

Haskett, S. E., Narahara, G. M., & Holditch, S. A. 1988. A method for simultaneous determination of permeability and porosity in low-permeability cores. *SPE formation evaluation*, 3(03), 651-658.

Hayek, M. 2015. Exact solutions for one-dimensional transient gas flow in porous media with gravity and Klinkenberg effects. *Transport in Porous Media*, 107(2), 403-417.

Hu, G., Wang, H., Fan, X., Yuan, Z., & Hong, S. 2009. Mathematical model of coalbed gas flow with Klinkenberg effects in multi-physical fields and its analytic solution. *Transport in Porous Media*, 76(3), 407.

Hu, T., Pang, X., Jiang, S., Wang, Q., Zheng, X., Ding, X., ... & Li, H. 2018. Oil content evaluation of lacustrine organic-rich shale with strong heterogeneity: A case study of the Middle Permian Lucaogou Formation in Jimusaer Sag, Junggar Basin, NW China. *Fuel*, 221, 196-205.

Hsieh, P. A., Tracy, J. V., Neuzil, C. E., Bredehoeft, J. D., & Silliman, S. E. 1981. A transient laboratory method for determining the hydraulic properties of 'tight' rocks—I. Theory. *In International Journal of Rock Mechanics and Mining Sciences & Geomechanics Abstracts* (Vol. 18, No. 3, pp. 245-252). Pergamon.

Innocentini, M. D., & Pandolfelli, V. C. 2001. Permeability of porous ceramics considering the Klinkenberg and inertial effects. *Journal of the American Ceramic Society*, 84(5), 941-944.

F. Javadpour, Nanopores and apparent permeability of gas flow in mudrocks (shales and siltstone), *J Can Petrol Technol* 48 (2009) 16–21.

Jones, S. C. 1997. A technique for faster pulse-decay permeability measurements in tight rocks. *SPE Formation Evaluation*, 12(01), 19-26.

Klinkenberg, L. J. 1941. The permeability of porous media to liquids and gases. In Drilling and production practice. *American Petroleum Institute*.

Kwon, O., Kronenberg, A. K., Gangi, A. F., & Johnson, B. 2001. Permeability of Wilcox shale and its effective pressure law. *Journal of Geophysical Research: Solid Earth*, 106(B9), 19339-19353.

Li, C., Xu, P., Qiu, S., & Zhou, Y. 2016. The gas effective permeability of porous media with Klinkenberg effect. *Journal of Natural Gas Science and Engineering*, 34, 534-540.

Liang, F., Sayed, M., Al-Muntasheri, G. A., Chang F. F., and Li, L. 2016. A comprehensive review on proppant technologies, *Petroleum*, 2(1): 26–39.

Ojala, I. O., & Fjær, E. 2007. The effective stress coefficient in porous sandstone. In 1st Canada-US Rock Mechanics Symposium. *American Rock Mechanics Association*.

Pang, Y., Soliman, M. Y., Deng, H., & Emadi, H. 2017. Analysis of effective porosity and effective permeability in shale-gas reservoirs with consideration of gas adsorption and stress effects. *SPE Journal*.

Soeder DJ. Porosity and permeability of eastern Devonian gas shale. *SPE Form Eval* 1988;3(2):116–24.

Vermylen, J. P. 2011. Geomechanical studies of the Barnett shale, Texas, USA. *Stanford University*.

Wang, G., Ren, T., Wang, K., & Zhou, A. 2014. Improved apparent permeability models of gas flow in coal with Klinkenberg effect. *Fuel*, 128, 53-61.

Warpinski, N. R., & Teufel, L. W. 1992. Determination of the effective-stress law for permeability and deformation in low-permeability rocks. *SPE formation evaluation*, 7(02), 123-131.

Worthington, P. F. 2004. The stress response of permeability. In SPE Annual Technical Conference and Exhibition. *Society of Petroleum Engineers.*

Wu, Y. S., & Pruess, K. 1998. Gas flow in porous media with Klinkenberg effects. *Transport in porous media*, 32(1), 117-137.

Ye, Z. and Ghassemi, A. 2016. Deformation Properties of Saw-Cut Fractures in Barnett, Mancos and Pierre Shales. Proceeeding: *50th US Rock Mechanics/Geomechanics Symposium, Houston, Texas.*

Zhang, J., Bai, M., Roegiers, J. C., Wang, J., & Liu, T. 2000. Experimental determination of stress-permeability relationship. In 4th North American Rock Mechanics Symposium. *American Rock Mechanics Association.*

Zhu, W. C., Liu, J., Sheng, J. C., & Elsworth, D. (2007). Analysis of coupled gas flow and deformation process with desorption and Klinkenberg effects in coal seams. *International Journal of Rock Mechanics and Mining Sciences*, 44(7), 971-980.